ACS NANO

www.acsnano.org

ARTICLE

Direct Growth of Vertical Graphene on Fiber Electrodes and Its Application in Alternating Current Line-Filtering Capacitors

Shichen Xu,[▽] Chao Shen,[▽] Zhisheng Peng, Jiandong Wu, Zhuo Chen, Xinyu Zhang, Nannan Ji, Muqiang Jian, Mingmao Wu,* Xin Gao,* and Jin Zhang*

Cite This: *ACS Nano* 2024, 18, 24154−24161

Read Online

ACCESS | Metrics & More | Article Recommendations | Supporting Information

ABSTRACT: **Fiber-shaped electrochemical capacitors (FSECs) have garnered substantial attention to emerging portable, flexible, and wearable electronic devices. However, achieving high electronic and ionic conductivity in fiber electrodes while maintaining a large specific surface area is still a challenge for enhancing the capacitance and rapid response of FSECs. Here, we present an electric-field-assisted cold-wall plasma-enhanced chemical vapor (EFCW-PECVD) method for direct growth of vertical graphene (VG) on fiber electrodes, which is incorporated in the FSECs. The customized reactor mainly consists of two radio frequency coils: one for plasma generation and the other for substrate heating. Precise temperature control can be achieved by adjusting the conductive plates and the applied power. With induction heating, only the substrate is heated to above 500 °C within just 5 min, maintaining a low temperature in the gas phase for the growth of VG with a high quality. Using this method, VG was easily grown on metallic fibers. The VG-coated titanium fibers for FSECs exhibit an ultrahigh rate performance and quick ion transport, enabling the conversion of an alternating current signal to a direct current signal and demonstrating outstanding filtering capabilities.**

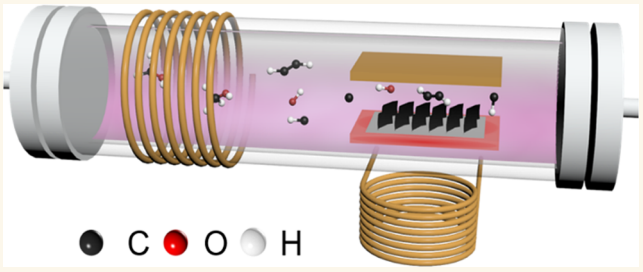

KEYWORDS: *vertical graphene, electric field, cold-wall method, fiber electrodes, line-filtering capacitors*

INTRODUCTION

High-frequency-response electrochemical capacitors (ECs), yielding the filtering capability of converting alternating current (AC) ripples into direct current (DC) signals, play an indispensable role in miniaturized, multifunctional, and high-power-density electronic systems.[1−6] Especially, with the rapid development of portable, flexible, and wearable electronic devices, fiber-shaped electrochemical capacitors (FSECs) have garnered substantial attention due to their appropriate flexibility and deformability as the fabric structures for energy storage.[7−12] Various fiber materials such as polymeric fibers[13,14] and metallic fibers,[15] as well as carbon nanotubes and graphene fibers, are extensively employed as electrode materials for ECs.[16] Nevertheless, a prevailing dilemma for most fiber electrodes resides in their structural contradictions, resulting in a situation where they either possess a restricted specific surface area or a smooth ion transport pathway.[8,9] This makes it challenging to simultaneously meet the requirements of high capacity and fast charge/discharge for electronic devices. Therefore, it is crucial to design special structures for fibers to enhance their electrochemical properties.

Vertical graphene (VG), as a typical three-dimensional (3D) material with abundant straight open channels and charge storage surfaces, has been widely used as electrode materials for electrochemical capacitors (ECs).[1,6,17−19] However, most of the vertical structures so far are constructed on the planar current collectors.[1,6,17−19] Therefore, it is highly important and meaningful to construct a VG structure on the fibers to fabricate high-performance FSECs. Differing from the physical methods of assembling VG using graphene oxide as structural units, plasma-enhanced chemical vapor deposition (PECVD) enables the direct and rapid growth of VG on various substrates, becoming the most principal method for the synthesis of VG.[20−22] However, PECVD is limited by its bulky and expensive equipment; even the commonly used radio

Received: April 25, 2024
Revised: August 8, 2024
Accepted: August 8, 2024
Published: August 20, 2024

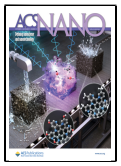

https://doi.org/10.1021/acsnano.4c05493
ACS Nano 2024, 18, 24154−24161

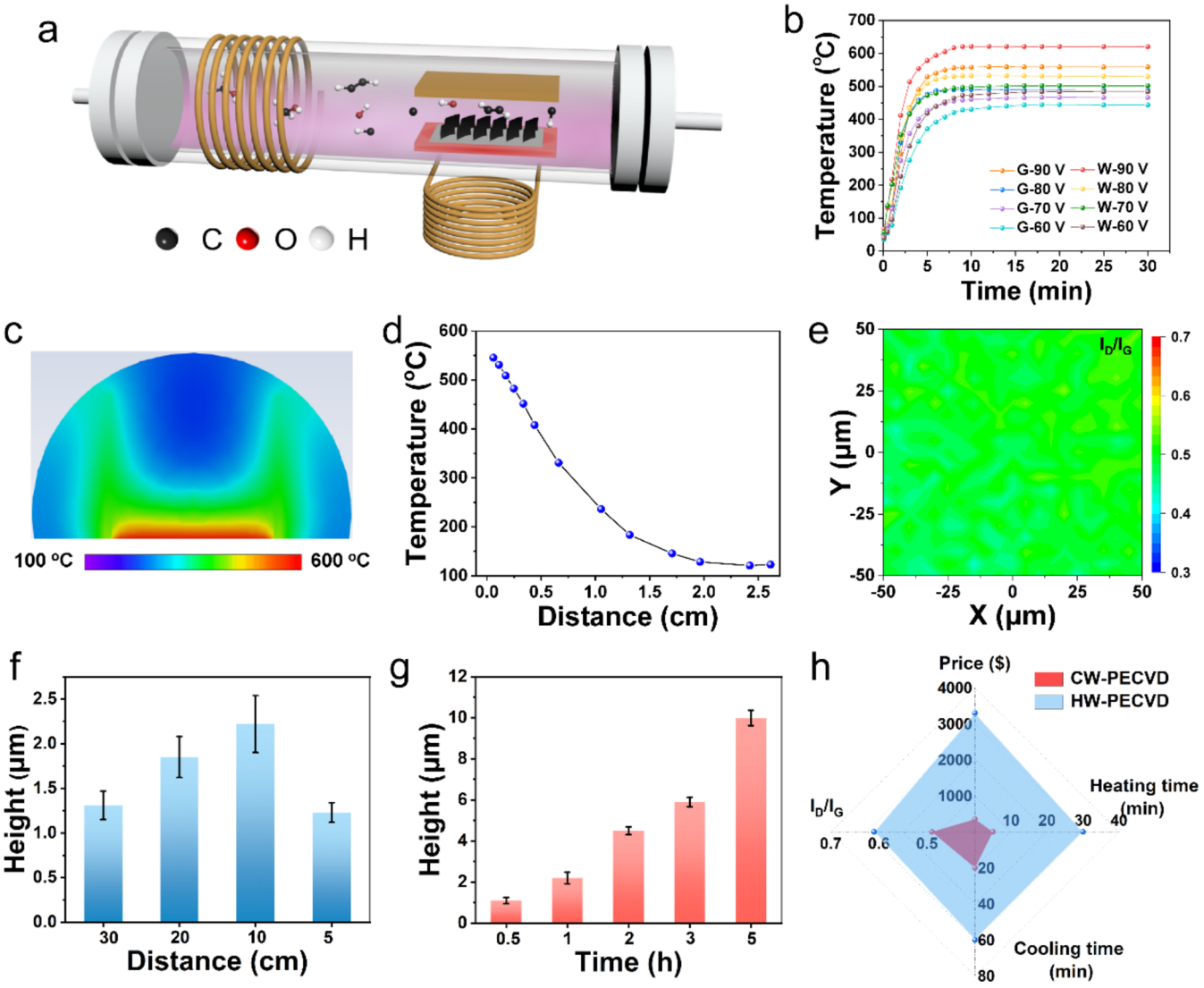

Figure 1. Homemade cold-wall PECVD system for VG growth. (a) Schematic of the homemade cold-wall PECVD system for the VG growth. (b) Plots of temperature versus induction heating time when using the graphite (G) plate and the tungsten (W) plate as the electrodes at different voltages. (c) Temperature simulation on the surface of the Si substrate during induction heating. (d) Temperature distribution along the vertical surface space of the Si substrate. (e) Raman mapping results of graphene grown on the Si wafer. (f) Height of VG varies with the distance between the two coils. (g) Height of VG versus growth time. (h) Comparison between cold-wall (CW) and hot-wall (HW) PECVD.

frequency PECVD (RF-PECVD) still requires a high-temperature heating furnace.[23−25] Therefore, it is crucial to search for simpler PECVD reaction equipment and more straightforward fabrication methods to grow VG on fibers.

Herein, we developed a cold-wall method for growing VG in an RF-PECVD system, which mainly consists of two sets of radio frequency induction coils. Not only rapid heating and cooling but also precise temperature control can be achieved using this homemade reactor. Moreover, only the substrate is easily heated to above 500 °C through induction heating while maintaining a low temperature in the gas phase, resulting in as-grown graphene with a high quality. As demonstrated by the Raman mapping results, the intensity ratio of I_D/I_G is 0.49 and I_{2D}/I_G is 0.91. Using this method, VG was grown on titanium fibers and then used as the electrodes. This FSEC exhibits good rate performances at a scan rate of 1000 V s^{-1} and great capacitance properties of 8.5 mF·cm^{-3} at 120 Hz, which outperforms most previously reported FSECs (the scan rate and frequency response typically being <100 V s^{-1} and 1 Hz). Moreover, the practical line-filtering performance for the conversion of the AC signal into the DC signal further confirmed the excellent VG structures with great potential for quick ion transport.

RESULTS AND DISCUSSION

Electric-Field-Assisted Cold-Wall PECVD Platform for VG Growth. As shown in Figure 1a, our homemade cold-wall PECVD system mainly contains two radio frequency copper coils; one wrapped around the quartz tube is used to generate plasma, while the other one placed below the quartz tube is used to heat the conductive plates inside the quartz tube. Methanol is introduced into the reaction system as the carbon source. Under the action of plasma, methanol undergoes decomposition and grows VG on the substrate. A built-in electric field was introduced into the reaction system to achieve the strictly vertical growth of graphene sheets, which

https://doi.org/10.1021/acsnano.4c05493
ACS Nano 2024, 18, 24154−24161

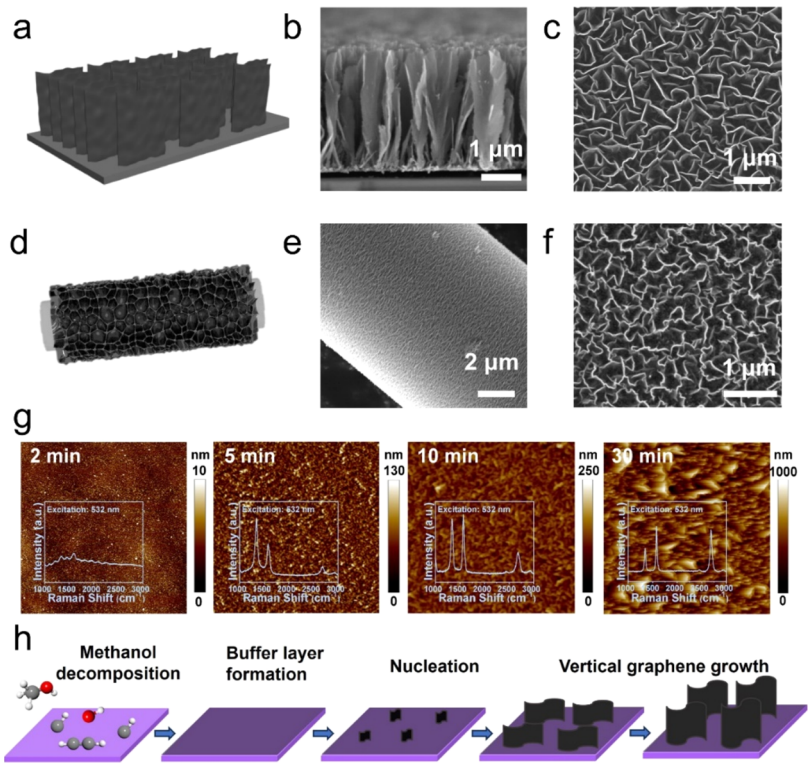

Figure 2. VG grown on different substrates by the cold-wall PECVD system and its formation process. (a) Schematic diagram of VG grown on the planar substrate. (b) Cross-sectional SEM of VG grown on the Si wafer. (c) Top-view SEM of VG grown on the Si wafer. (d) Schematic diagram of VG grown on the fiber substrate. (e) SEM image of VG grown on the Ti fiber. (f) Top-view SEM of VG grown on the Ti fiber. (g) AFM images of VG grown within 2, 5, 10, and 30 min, respectively. The inset pictures are the Raman spectra. (h) Schematic of the formation process for VG nanosheets.

was generated by two electrodes put inside the quartz tube and connected to a direct current power supply. The substrate for growing VG is placed on the lower electrode, and then a thermocouple is placed on the substrate to monitor the temperature in real time. It is important to emphasize that the temperature of the electrode plate being induction-heated is dependent on the output power and the electrode material (Figure S1). When the graphite paper is used as the electrode and an applied voltage is 90 V, the matched current is 60 A. With the increasing induction heating time, the temperature on the substrate surface rapidly increases within 2 min and stabilizes after 5 min. Finally, the substrate reached 550 °C (Figure 1b). Combining air cooling and water cooling, the reaction system can be cooled to room temperature within 20 min. In addition, as the applied power increases, the heating rate also increases. A higher temperature was achieved by replacing the graphite electrode with the high-melting-point tungsten electrode, which has a high electrical conductivity (Figure 1b).

The temperature is critical for both the decomposition of the carbon source in the gas phase and the growth of VG on the substrate. We used the COMSOL simulation to analyze the temperature of the cold-walled PECVD system. The results show that the temperature gradually decreases in the vertical direction of the substrate (Figure 1c). When the temperature of the substrate was 550 °C, the temperature in the space 1 cm away from the substrate is below 250 °C (Figure 1d), which indicated that only the surface of the substrate has a sufficiently high temperature for further decomposition of the carbon source to grow VG. The lower temperature in the gas phase prevents high-energy plasma from generating complex carbon species, thereby reducing the possibility of formation of amorphous carbon on VG. This also results in a good conductivity of grown vertical graphene (Figure S2). As-prepared VG using the cold-wall PECVD method exhibits a good uniformity as well as a low average I_D/I_G of 0.49 and a high average I_{2D}/I_G of 0.91 (Figure 1e, Figure S3).

The growth rate is dependent not only on the reaction temperature but also on the density of plasma. To analyze how the density of plasma affects VG growth, we adjusted the distance between the reaction substrate and the plasma generator. When the power applied to the plasma generator is constant, the density of plasma around the substrate surface is related to the distance between the substrate and the plasma generator. As the distance decreased, the density of plasma increased, and thus, the growth rate of VG is increased. When the distance is 10 cm, VG exhibits the fastest growth rate of 2.2 $\mu m \cdot h^{-1}$ (Figure 1f). However, when the plasma density is higher than the threshold (Figure S4, the distance is 5 cm), the stronger plasma has an etching effect that is detrimental to the growth of VG. In addition, the height of VG increases with an increase in growth time (Figure S5). VG with a height of 10 μm was synthesized for 5 h (Figure 1g). We compare our EFCW-PECVD synthesis platform with reported PECVD for VG growth, showing the exciting combination of very high heating/cooling rates, low price, and high-quality VG growth in our platform (Figure 1h and Table S1).

Moreover, the use of induction heating greatly shortens the heating and cooling times. When using a conventional CVD tube furnace, considering the protection of the resistance wire, it usually takes 20 to 30 min to raise the temperature to 600 °C and at least 1 h to lower the temperature to room temperature.

https://doi.org/10.1021/acsnano.4c05493
ACS Nano 2024, 18, 24154−24161

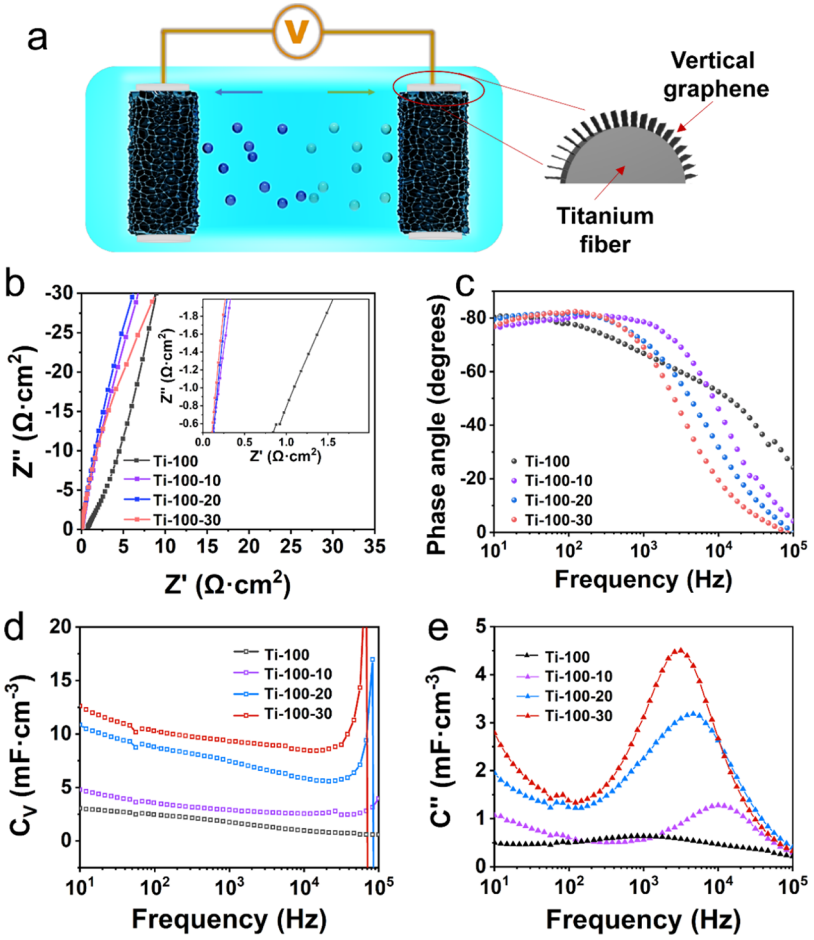

Figure 3. Electrochemical performance of FSECs based on the Ti fiber with and without VG. (a) Schematic of FSECs based on the VG-coated fiber. (b) Nyquist plot; inset: the expanded view at high frequencies. (c) Bode diagrams (frequency versus phase angle) of FSEC-Ti_f. (d) Frequency dependences of the volumetric capacitances (CVs) of FSEC-Ti_f. (e) Plots of imaginary capacitances (C'') versus frequency.

In contrast, our method only takes 5 min to raise the temperature to the desired level and within 20 min to lower it to room temperature. The higher the target temperature, the more pronounced are the advantages of induction heating. In addition, the CW system can significantly improve the quality of graphene, yielding a lower I_D/I_G than VG grown in HW-PECVD (Figure S6).

Direct Growth of VG on Various Substrates Using the EFCW-PECVD Platform. With the EFCW-PECVD synthesis platform, we demonstrate that VG can be synthesized on different dimensional substrates. Here, we synthesized VG on a silicon wafer (2D) and a titanium fiber (1D). When a voltage of 100 V was applied to two electrodes, an electric field of 66.67 $V{\cdot}cm^{-1}$ was induced to assist the directional growth of VG. As shown in the schematic diagram (Figure 2a) and the sectional-view scanning electron microscopy (SEM) image (Figure 2b), graphene sheets strictly perpendicular to the substrate were synthesized within 1 h, which is totally different from the morphology of VG grown without an electric field (Figure S7). In the top-view SEM, only a linelike morphology can be seen, indicating that graphene is strictly perpendicular to the substrate (Figure 2c). In addition to growing VG on planar substrates, it can also be achieved on small-area substrates with curved surfaces (1D substrates). Figure 2d shows a schematic of vertically aligned graphene on a fiber substrate. The surface of the titanium fiber substrate is coated with a layer of graphene material after 30 min growth (Figure 2e). SEM images of graphene grown on the fiber surface reveal a linear morphology, indicating that graphene grows vertically (Figure 2f). The transmission electron microscopy (TEM) image (Figure S8) reveals the morphology of parallel-aligned graphene sheets with a lateral dimension of up to 2 μm. Few-layered graphene sheets were observed in the high-resolution TEM of VG arrays, and the interlayer spacing for few-layered graphene was ~0.34 nm (Figure S9). High-resolution TEM images show a buffer layer composed of amorphous carbon between the substrate and the graphene layers (Figure S10).

Concerning the growing mechanism of VG using the cold-wall PECVD synthesis, we use atomic force microscopy (AFM) and Raman spectroscopy to trace the growth process (Figure 2g), and a feasible mechanism of the process can be proposed (Figure 2h). It can be observed that there is a buffer layer formation and a nucleation stage lasting at least 2 min. VG begins to appear on the substrate within 5 min, and the Raman spectrum shows the characteristic G band and 2D band of graphene. As the induction heating time increases, VG gradually grows larger and denser on the substrate (Figure S11).

VG on Fiber Electrodes for Fiber-Shaped Electrochemical Capacitors (FSECs). With abundant channels and high surface areas for charge storage (Figure S12), VG on the Ti fiber is believed to exhibit a superior high-rate FSEC

https://doi.org/10.1021/acsnano.4c05493
ACS Nano 2024, 18, 24154−24161

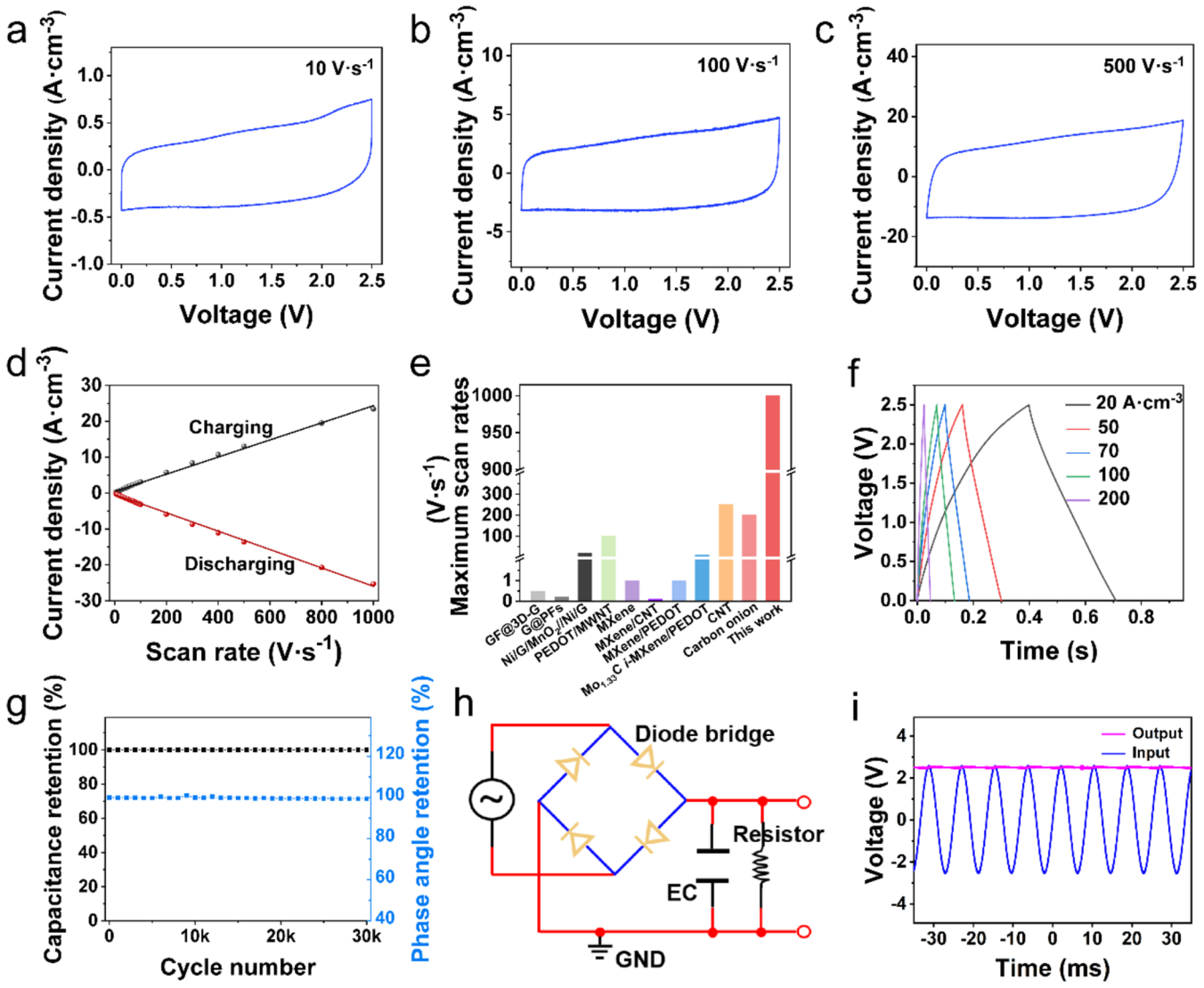

Figure 4. Rate capability and filtering performances of FSECs based on the VG-coated Ti fiber. CV curves of FSEC-Ti$_{20}$ tested with scan rates at (a)10, (b) 100, and (c) 500 V·s^{-1}. (d) Plots of charge/discharge current density versus scan rate. (e) Comparation of charge/discharge rates between FSEC-Ti$_{20}$ and other FSECs. (f) Galvanostatic charge−discharge curves at various current densities. (g) Cycling stability of FSEC-Ti$_{20}$. (h) Schematic of the circuit used for smoothing AC signals. (i) Filtering performance of FSEC-Ti$_{20}$.

performance. The schematic of FSECs based on VG-coated fibers is shown in Figure 3a. Concretely, the symmetric FSEC was fabricated by two identical Ti fiber electrodes and sealed on a plastic sheet with 1 M acetonitrile solution of tetraethylammonium-tetrafluoroborate as the electrolyte. Ti wires (100 μm in diameter) were used as the electrodes to ensure the electrochemical stability. Notably, FSEC-Ti$_t$ is used to represent the FSEC based on different Ti fibers, where t means the growth time of VG arrays, including 0, 10, 20, and 30 min.

For analysis of the electrochemical performances of FSEC-Ti$_t$, the electrochemical impedance spectroscopy (EIS) measurements were performed to provide their frequency dependence characteristics. In the Nyquist plots, all of the curves of FSEC-Ti$_t$ exhibit an imaginary impedance (Z'') almost vertical to the real axis and an absence of the semicircle at the high-frequency region, indicating an excellent capacitive behavior of high-quality VG rather than the faradaic charge transfer reaction (Figure 3b). Additionally, FSEC-Ti$_{10}$, FSEC-Ti$_{20}$, and FSEC-Ti$_{30}$ exhibit extremely small equivalent series resistances around 0.07 Ω·cm^2, implying the firm contact between VG and the Ti fiber. The Bode diagrams (frequency versus phase angle) of FSEC-Ti$_t$ depict the frequency response capability. Generally, ideal capacitive devices with a fast response will have a phase angle closer to −90° at higher frequencies. FSEC-Ti$_0$, FSEC-Ti$_{10}$, FSEC-Ti$_{20}$, and FSEC-Ti$_{30}$ realize phase angles below −80° when the frequencies were 32, 560, 275, and 259 Hz, respectively (Figure 3c). Among them, fiber electrodes with VG arrays can realize faster frequencies because of the better wettability of carbon materials in organic electrolytes than pure Ti fibers. Meanwhile, with the growth time decrease, FSEC-Ti$_t$ exhibits the faster frequency response capability, which is attributed to the quicker ion transport in the thinner VG electrode materials. Furthermore, at a "factor of merit" frequency of 120 Hz, which is usually used to estimate practical applications of capacitors such as AC line-filtering capacitors, FSEC-Ti$_{10}$, FSEC-Ti$_{20}$, and FSEC-Ti$_{30}$, all show a phase angle approaching −81°, indicating their excellent high-frequency response.

https://doi.org/10.1021/acsnano.4c05493
ACS Nano 2024, 18, 24154−24161

The frequency dependences of the volumetric capacitances (C_V) of FSEC-Ti$_t$ are given in Figure 3d. With the growth time increase, the C_V of FSEC-Ti$_0$, FSEC-Ti$_{10}$, FSEC-Ti$_{20}$, and FSEC-Ti$_{30}$ exhibits an increasing trend at the whole frequency range. It is owing to the fact that the thicker VG thickness will add ionic adsorption sites and offer a higher capacitance density. Specifically, at 120 Hz, the C_V values of FSEC-Ti$_0$, FSEC-Ti$_{10}$, FSEC-Ti$_{20}$, and FSEC-Ti$_{30}$ were calculated to be 2.7, 3.4, 8.5, and 10 mF·cm^{-3}, respectively. It should be noted that the volume of FSEC-Ti$_t$ includes two titanium wire electrodes during the calculation of C_V. In addition, the specific areal capacitance of FSEC-Ti$_t$ is also better than that of FSEC-Ti (Figure S13). Besides, the complex model of the capacitance was plotted versus the frequency (Figure 3e). The characteristic frequency (f_0) defines the relaxation time constant ($\tau_0 = 1/f_0$) that could be read out at the maximum C''. The τ_0 values of FSEC-Ti$_{10}$, FSEC-Ti$_{20}$, and FSEC-Ti$_{30}$ are 0.099, 0.215, and 0.316 ms, respectively, implying a quick ion adsorption/desorption process of the fiber electrodes. More importantly, all of these good properties can also be found when the diameter of the Ti fiber is 200 μm (Figure S14).

We further conducted cyclic voltammetry (CV) tests to confirm the high-rate capability of FSEC-Ti$_t$. The FSEC-Ti$_{20}$ sample was selected as an example for analysis. The CV profiles of FSEC-Ti$_{20}$ under progressively increasing scan rates, reaching up to 1000 V·s^{-1}, are shown in Figures 4a–c and S15. Even at such rapid charge/discharge rates, the CV profiles exhibited quasi-rectangular shapes, validating its good capacitive behavior, which is different from that of FSEC-Ti (Figure S16). Furthermore, a good linear correlation was observed between the charge/discharge current density and the scan rate within the range from 10 to 1000 V·s^{-1} (Figure 4d), also indicating the absence of hysteresis during the charge–discharge process. It is worth mentioning that the achieved scan rate of 1000 V·s^{-1} represents an exceptionally high value compared to most carbon-based FSECs reported to date (Figure 4e and Table S2).[26−35] Moreover, the galvanostatic charge–discharge (GCD) curves of FSEC-Ti$_{20}$ exhibit quasi-isosceles triangular shapes as the current density is incremented from 20 to 200 A·cm^{-3}, further substantiating its ultrahigh rate performance (Figure 4f). FSEC-Ti$_{20}$ also possesses great electrochemical stability and durability when subjected to continuous high-rate testing. Even after undergoing 30,000 cycles of charging and discharging at a rate of 10 V s^{-1}, the retention of the capacitance and phase angle at 120 Hz remains nearly 100%, indicating an excellent long-term performance (Figure 4g).

Finally, with the ultrahigh frequency response capability and excellent capacitive behaviors of the VG arrays, the practical ripple filtering performance was tested. FSEC-Ti$_{20}$ was incorporated in an experimental model of AC/DC conversion (Figure 4h), which includes a full-wave bridge rectifier, a filter capacitor (FSEC-t), and a resistor (R = 1 MΩ). Figure 4i presents the ripple filtering demonstration of single FSEC-Ti$_{20}$ under a sinusoidal input signal (V_{peak} = ±2.5 V, 60 Hz). The output signal could be a smooth straight line, suggesting rapid ion transport kinetics owing to the excellent vertical structure on the fiber surfaces.

CONCLUSIONS

In conclusion, this study designed a cold-wall PECVD system, which not only allows for the growth of VG perpendicular to the substrate by coupling with an electric field but also enables the growth of VG at a low temperature. In addition, VG-coated Ti fibers as electrodes for FSECs exhibit ultrafast rate performances and great capacitance properties. The FSECs showed excellent C_V values and a phase angle at 120 Hz with arbitrary AC filtering performances, which is better than most of the reported fiber-based electrochemical capacitors. This work demonstrated the colossal promising potential of VG on fiber electrodes in wearable electronic devices.

METHOD/EXPERIMENTAL SECTION

Growth of VG Arrays with Cold-Wall PECVD. The cold-wall PECVD system mainly contains two radio frequency copper coils; the one wrapped around the quartz tube is used to generate plasma, while the other one placed below the quartz tube is used to induce heating in the conductive plates inside the quartz tube. The electric field was provided by two electrodes connected to a direct current power supply. The voltage can be adjusted easily. In brief, a 2 × 2 × 0.05 cm^3 silicon wafer with a 300-nanometer oxide layer after cleaning was placed on the lower electrode as the substrate. Plasma was then generated with a radio frequency source power of 250 W. After that, a carbon source such as methanol was introduced into the system. After turning on the button of the water-cooled chiller, the voltage of the power supply was adjusted to the impedance matching device. Then, the copper coil could inductively heat the electrode in the quartz tube. Finally, VG was grown on the substrate. When an electric field was introduced into the system, oriented VG arrays could be obtained on the substrate. Just by replacing the titanium fiber with the silicon wafer, VG can be grown on the titanium fiber.

Assembly of the FSEC. Two of the same fiber electrodes were positioned in a parallel configuration upon a polyethylene glycol terephthalate (PET) plastic. The two electrodes were then secured in place by clamps. Following this, the edges of the PET sheet were enveloped by a double-sided tape (3 M VHB). These tapes served the dual purpose of firmly affixing the fibrous electrodes while maintaining a separation distance of ∼2 mm between them. Subsequently, 5 μL of 1 M acetonitrile solution of tetraethylammonium-tetrafluoroborate electrolyte was added on two fibrous electrodes. Finally, with another PET sheet covering the double-sided tape, one FSEC device was fabricated.

Electrochemical Characterization. The electrochemical characterizations were performed on a CHI 660E workstation (CH Instruments Inc., China). For CV and GCD studies, the window voltages were set from 0 to 2.5 V. EIS tests were conducted at 5 mV amplitude in the frequency range of 1–100 000 Hz.

The specific areal capacitance (C_A) of the FSEC was calculated by

$$C_A = -\frac{1}{2\pi f Z'' S} \tag{1}$$

The specific volumetric capacitance (C_V) of the FSEC was calculated by

$$C_V = -\frac{1}{2\pi f Z'' V} \tag{2}$$

The real specific areal capacitance (C') was calculated by

$$C' = -\frac{Z''}{2\pi f |Z|^2 S} \tag{3}$$

The imaginary specific areal capacitance (C'') was calculated by

$$C'' = \frac{Z'}{2\pi f |Z|^2 S} \tag{4}$$

The τ_0 was derived from the f_o at maximum C''

$$\tau_0 = \frac{1}{f_0} \tag{5}$$

where f is the frequency; Z' or Z'' is the real or imaginary impedance; Z is the total impedance; S is the frontal projected area of the two

https://doi.org/10.1021/acsnano.4c05493
ACS Nano 2024, 18, 24154−24161

fiber electrodes; V is the volume of the two fiber electrodes, including the metal fibers and graphene; and f_0 is the frequency at maximum C''.

Characterization. The morphology and detailed structure of VG was investigated by SEM (FEI Quattro S; acceleration voltage 5−20 kV), TEM (FEI Tecnai F20; acceleration voltage 200 kV), aberration-corrected atomic-resolved TEM (Titan Cubed Themis G2 300; 200 kV), Raman spectroscopy (Horiba, LabRAM HR 800; 532 nm laser wavelength), and XPS (Kratos Analytical Axis-Ultra spectrometer with an Al Kα X-ray source). The AC line-filtering performances were tested using a 33511B arbitrary function generator (Agilent Technologies Inc., Tektronix) and a GBPC3005W readymade single-phase silicon bridge rectifier (Sep Electron. Corp., Taibei, China). All of the outputs were recorded on a RTB2002 mixed domain oscilloscope (Rohde & Schwarz, Germany).

ASSOCIATED CONTENT

Supporting Information

The Supporting Information is available free of charge at https://pubs.acs.org/doi/10.1021/acsnano.4c05493.

SEM images, TEM images, Raman spectra, and other graphs and data (PDF)

AUTHOR INFORMATION

Corresponding Authors

Mingmao Wu − *Key Laboratory of Advanced Materials Technologies, International (HongKong Macao and Taiwan) Joint Laboratory on Advanced Materials Technologies, College of Materials Science and Engineering, Fuzhou University, Fuzhou 350108, P. R. China;* orcid.org/0000-0002-6942-7702; Email: wumm20@fzu.edu.cn

Xin Gao − *School of Materials Science and Engineering, Peking University, Beijing 100871, P. R. China; Beijing Graphene Institute (BGI), Beijing 100095, P. R. China;* orcid.org/0000-0001-5360-0796; Email: gaoxin-cnc@pku.edu.cn

Jin Zhang − *Beijing Science and Engineering Center for Nanocarbons, Beijing National Laboratory for Molecular Sciences, College of Chemistry and Molecular Engineering, Peking University, Beijing 100871, P. R. China; School of Materials Science and Engineering, Peking University, Beijing 100871, P. R. China; Beijing Graphene Institute (BGI), Beijing 100095, P. R. China;* orcid.org/0000-0003-3731-8859; Email: jinzhang@pku.edu.cn

Authors

Shichen Xu − *Beijing Science and Engineering Center for Nanocarbons, Beijing National Laboratory for Molecular Sciences, College of Chemistry and Molecular Engineering, Peking University, Beijing 100871, P. R. China; School of Materials Science and Engineering, Peking University, Beijing 100871, P. R. China; Beijing Graphene Institute (BGI), Beijing 100095, P. R. China*

Chao Shen − *Beijing Graphene Institute (BGI), Beijing 100095, P. R. China; College of Chemistry and Chemical Engineering, Ningxia University, Yinchuan 750021, P. R. China*

Zhisheng Peng − *School of Materials Science and Engineering, Peking University, Beijing 100871, P. R. China*

Jiandong Wu − *College of Engineering, Peking University, Beijing 100871, P. R. China*

Zhuo Chen − *Beijing Science and Engineering Center for Nanocarbons, Beijing National Laboratory for Molecular Sciences, College of Chemistry and Molecular Engineering, Peking University, Beijing 100871, P. R. China; Beijing Graphene Institute (BGI), Beijing 100095, P. R. China*

Xinyu Zhang − *Beijing Science and Engineering Center for Nanocarbons, Beijing National Laboratory for Molecular Sciences, College of Chemistry and Molecular Engineering, Peking University, Beijing 100871, P. R. China; Beijing Graphene Institute (BGI), Beijing 100095, P. R. China*

Nannan Ji − *Beijing Graphene Institute (BGI), Beijing 100095, P. R. China*

Muqiang Jian − *Beijing Graphene Institute (BGI), Beijing 100095, P. R. China*

Complete contact information is available at: https://pubs.acs.org/10.1021/acsnano.4c05493

Author Contributions

$^{\nabla}$S.C.X. and C.S. contributed equally to this work.

Notes

The authors declare no competing financial interest.

ACKNOWLEDGMENTS

This work was financially supported by the Ministry of Science and Technology of China (2022YFA1203302 and 2022YFA1203304), the National Natural Science Foundation of China (Grant Nos. T2188101, 52021006, 52302034), the Strategic Priority Research Program of CAS (XDB36030100), the Beijing National Laboratory for Molecular Sciences (BNLMS-CXTD-202001), the Shenzhen Science and Technology Innovation Commission (KQTD20221101115627004), and the Natural Science Foundation of Fujian Province of China (2021J01588).

REFERENCES

(1) Miller, J. R.; Outlaw, R. A.; Holloway, B. C. Graphene Double-Layer Capacitor with ac Line-Filtering Performance. *Science* **2010**, *329*, 1637−1639.

(2) Wu, Z. S.; Liu, Z.; Parvez, K.; Feng, X.; Mullen, K. Ultrathin Printable Graphene Supercapacitors with AC Line-Filtering Performance. *Adv. Mater.* **2015**, *27*, 3669−3675.

(3) Zhang, M.; Zhou, Q.; Chen, J.; Yu, X.; Huang, L.; Li, Y.; Li, C.; Shi, G. An ultrahigh-rate electrochemical capacitor based on solution-processed highly conductive PEDOT:PSS films for AC line-filtering. *Energy Environ. Sci.* **2016**, *9*, 2005−2010.

(4) Chi, F.; Li, C.; Zhou, Q.; Zhang, M.; Chen, J.; Yu, X.; Shi, G. Graphene-Based Organic Electrochemical Capacitors for AC Line Filtering. *Adv. Energy Mater.* **2017**, *7*, No. 1700591.

(5) Gund, G. S.; Park, J. H.; Harpalsinh, R.; Kota, M.; Shin, J. H.; Kim, T.-i.; Gogotsi, Y.; Park, H. S. MXene/Polymer Hybrid Materials for Flexible AC-Filtering Electrochemical Capacitors. *Joule* **2019**, *3*, 164−176.

(6) Wu, M.; Chi, F.; Geng, H.; Ma, H.; Zhang, M.; Gao, T.; Li, C.; Qu, L. Arbitrary waveform AC line filtering applicable to hundreds of volts based on aqueous electrochemical capacitors. *Nat. Commun.* **2019**, *10*, No. 2855.

(7) Wu, M.; Sun, K.; He, J.; Huang, Q.; Zhan, W.; Lu, Z.; Xia, M. C.; Zhang, Y.; Lyu, X.; Geng, H.; Luo, Z. Z.; Zou, Z. Hierarchically 3D Fibrous Electrode for High-Performance Flexible AC-Line Filtering in Fluctuating Energy Harvesters. *Adv. Funct. Mater.* **2023**, *33*, No. 2305039.

(8) Chen, D.; Jiang, K.; Huang, T.; Shen, G. Recent Advances in Fiber Supercapacitors: Materials, Device Configurations, and Applications. *Adv. Mater.* **2020**, *32*, No. e1901806.

(9) Lee, J.; Llerena Zambrano, B.; Woo, J.; Yoon, K.; Lee, T. Recent Advances in 1D Stretchable Electrodes and Devices for Textile and Wearable Electronics: Materials, Fabrications, and Applications. *Adv. Mater.* **2020**, *32*, No. e1902532.

(10) Kim, B. C.; Hong, J. Y.; Wallace, G. G.; Park, H. S. Recent Progress in Flexible Electrochemical Capacitors: Electrode Materials, Device Configuration, and Functions. *Adv. Energy Mater.* **2015**, *5*, No. 1500959.
(11) Gao, K.; Wang, S.; Liu, W.; Yue, Y.; Rao, J.; Su, J.; Li, L.; Zhang, Z.; Liu, N.; Xiong, L.; Gao, Y. All Fiber Based Electrochemical Capacitor towards Wearable AC Line Filters with Outstanding Rate Capability. *ChemElectroChem.* **2019**, *6*, 1450−1457.
(12) Fakharuddin, A.; Li, H.; Di Giacomo, F.; Zhang, T.; Gasparini, N.; Elezzabi, A. Y.; Mohanty, A.; Ramadoss, A.; Ling, J.; Soultati, A.; Tountas, M.; Schmidt-Mende, L.; Argitis, P.; Jose, R.; Nazeeruddin, M. K.; Mohd Yusoff, A. R. B.; Vasilopoulou, M. Fiber-Shaped Electronic Devices. *Adv. Energy Mater.* **2021**, *11*, No. 2101443.
(13) Wu, Q.; Xu, Y.; Yao, Z.; Liu, A.; Shi, G. Supercapacitors Based on Flexible Graphene/Polyaniline Nanofiber Composite Films. *ACS Nano* **2010**, *4*, 1963−1970.
(14) Bae, J.; Song, M. K.; Park, Y. J.; Kim, J. M.; Liu, M.; Wang, Z. L. Fiber supercapacitors made of nanowire-fiber hybrid structures for wearable/flexible energy storage. *Angew. Chem., Int. Ed.* **2011**, *50*, 1683−1687.
(15) Li, P.; Li, J.; Zhao, Z.; Fang, Z.; Yang, M.; Yuan, Z.; Zhang, Y.; Zhang, Q.; Hong, W.; Chen, X.; Yu, D. A General Electrode Design Strategy for Flexible Fiber Micro-Pseudocapacitors Combining Ultrahigh Energy and Power Delivery. *Adv. Sci.* **2017**, *4*, No. 1700003.
(16) Zhao, J.; Zhang, Y.; Yan, J.; Zhao, X.; Xie, J.; Luo, X.; Peng, J.; Wang, J.; Meng, L.; Zeng, Z.; Lu, C.; Xu, X.; Dai, Y.; Yao, Y. Fiber-Shaped Electrochemical Capacitors Based on Plasma-Engraved Graphene Fibers with Oxygen Vacancies for Alternating Current Line Filtering Performance. *ACS Appl. Energy Mater.* **2019**, *2*, 993−999.
(17) Cai, M.; Outlaw, R. A.; Butler, S. M.; Miller, J. R. A high density of vertically-oriented graphenes for use in electric double layer capacitors. *Carbon* **2012**, *50*, 5481−5488.
(18) Miller, J. R.; Outlaw, R. A. Vertically-Oriented Graphene Electric Double Layer Capacitor Designs. *J. Electrochem. Soc.* **2015**, *162*, A5077−A5082.
(19) Xu, S.; Wen, Y.; Chen, Z.; Ji, N.; Zou, Z.; Wu, M.; Qu, L.; Zhang, J. Vertical Graphene Arrays as Electrodes for Ultra-High Energy Density AC Line-Filtering Capacitors. *Angew. Chem., Int. Ed.* **2021**, *60*, 24505−24509.
(20) Bo, Z.; Yang, Y.; Chen, J.; Yu, K.; Yan, J.; Cen, K. Plasma-enhanced chemical vapor deposition synthesis of vertically oriented graphene nanosheets. *Nanoscale* **2013**, *5*, 5180−5204.
(21) Yi, K.; Liu, D.; Chen, X.; Yang, J.; Wei, D.; Liu, Y.; Wei, D. Plasma-enhanced chemical vapor deposition of two-dimensional materials for applications. *Acc. Chem. Res.* **2021**, *54*, 1011−1022.
(22) Han, Z. J.; Murdock, A. T.; Seo, D. H.; Bendavid, A. Recent progress in plasma-assisted synthesis and modification of 2D materials. *2D Mater.* **2018**, *5*, No. 032002.
(23) Shiji, K.; Hiramatsu, M.; Enomoto, A.; Nakamura, M.; Amano, H.; Hori, M. Vertical growth of carbon nanowalls using rf plasma-enhanced chemical vapor deposition. *Diam. Relat. Mater.* **2005**, *14*, 831−834.
(24) Sato, G.; Morio, T.; Kato, T.; Hatakeyama, R. Fast Growth of Carbon Nanowalls from Pure Methane using Helicon Plasma-Enhanced Chemical Vapor Deposition. *Jpn. J. Appl. Phys.* **2006**, *45*, 5210−5212.
(25) Kondo, S.; Hori, M.; Yamakawa, K.; Den, S.; Kano, H.; Hiramatsu, M. Highly reliable growth process of carbon nanowalls using radical injection plasma-enhanced chemical vapor deposition. *J. Vac. Sci. Technol. B* **2008**, *26*, 1294−1300.
(26) Meng, Y.; Zhao, Y.; Hu, C.; Cheng, H.; Hu, Y.; Zhang, Z.; Shi, G.; Qu, L. All-graphene core-sheath microfibers for all-solid-state, stretchable fibriform supercapacitors and wearable electronic textiles. *Adv. Mater.* **2013**, *25*, 2326−2331.
(27) Lee, J. A.; Shin, M. K.; Kim, S. H.; Cho, H. U.; Spinks, G. M.; Wallace, G. G.; Lima, M. D.; Lepro, X.; Kozlov, M. E.; Baughman, R. H.; Kim, S. J. Ultrafast charge and discharge biscrolled yarn supercapacitors for textiles and microdevices. *Nat. Commun.* **2013**, *4*, No. 1970.
(28) Padmajan Sasikala, S.; Lee, K. E.; Lim, J.; Lee, H. J.; Koo, S. H.; Kim, I. H.; Jung, H. J.; Kim, S. O. Interface-Confined High Crystalline Growth of Semiconducting Polymers at Graphene Fibers for High-Performance Wearable Supercapacitors. *ACS Nano* **2017**, *11*, 9424−9434.
(29) Yu, C.; Gong, Y.; Chen, R.; Zhang, M.; Zhou, J.; An, J.; Lv, F.; Guo, S.; Sun, G. A Solid-State Fibriform Supercapacitor Boosted by Host-Guest Hybridization between the Carbon Nanotube Scaffold and MXene Nanosheets. *Small* **2018**, *14*, No. e1801203.
(30) Jha, M. K.; Ball, R.; Seelaboyina, R.; Subramaniam, C. All Solid-State Coaxial Supercapacitor with Ultrahigh Scan Rate Operability of 250 000 mV/s by Thermal Engineering of the Electrode−Electrolyte Interface. *ACS Appl. Energy Mater.* **2020**, *3*, 3454−3464.
(31) Pech, D.; Brunet, M.; Durou, H.; Huang, P.; Mochalin, V.; Gogotsi, Y.; Taberna, P. L.; Simon, P. Ultrahigh-power micrometre-sized supercapacitors based on onion-like carbon. *Nat. Nanotechnol.* **2010**, *5*, 651−654.
(32) Liu, W.; Feng, K.; Zhang, Y.; Yu, T.; Han, L.; Lui, G.; Li, M.; Chiu, G.; Fung, P.; Yu, A. Hair-based flexible knittable supercapacitor with wide operating voltage and ultra-high rate capability. *Nano Energy* **2017**, *34*, 491−499.
(33) Qin, L.; Jiang, J.; Hou, L.; Zhang, F.; Rosen, J. MXene-based multifunctional smart fibers for wearable and portable electronics. *J. Mater. Chem. A* **2022**, *10*, 12544−12550.
(34) Zhang, J.; Uzun, S.; Seyedin, S.; Lynch, P. A.; Akuzum, B.; Wang, Z.; Qin, S.; Alhabeb, M.; Shuck, C. E.; Lei, W.; Kumbur, E. C.; Yang, W.; Wang, X.; Dion, G.; Razal, J. M.; Gogotsi, Y. Additive-Free MXene Liquid Crystals and Fibers. *ACS Cent. Sci.* **2020**, *6*, 254−265.
(35) Zhang, J.; Seyedin, S.; Qin, S.; Wang, Z.; Moradi, S.; Yang, F.; Lynch, P. A.; Yang, W.; Liu, J.; Wang, X.; Razal, J. M. Highly Conductive $Ti_3C_2T_x$ MXene Hybrid Fibers for Flexible and Elastic Fiber-Shaped Supercapacitors. *Small* **2019**, *15*, No. e1804732.

https://doi.org/10.1021/acsnano.4c05493
ACS Nano 2024, 18, 24154−24161